



Value-added biocarbon production through slow pyrolysis of mixed bio-oil wastes: studies on their physicochemical characteristics and structure–property–processing co-relation

Ranjeet Kumar Mishra¹ · Manjusri Misra^{1,2} · Amar K. Mohanty^{1,2}

Received: 15 March 2022 / Revised: 30 May 2022 / Accepted: 1 June 2022 / Published online: 8 July 2022
© The Author(s) 2022

Abstract

In this work, mixed bio-oil (MBO) is transformed into valuable biocarbon through slow pyrolysis technique. MBO was accomplished in a semi-batch reactor at 600 and 900 °C temperature, 10 °C min⁻¹ heating rate, and 30 min holding time under a non-oxidizing environment. The produced mixed bio-oil-derived biocarbon (MBOB) was characterized by its surface properties, thermal stability, elemental composition, thermal conductivity, BET surface area, surface morphology, and electrical conductivity. The pyrolysis outcomes established that the temperature has a predominant impact on the variation in yield and properties of MBOB. Characterization results of MBOB exposed increased properties (thermal stability, electrical and thermal conductivity, graphitic content, carbon content, and HHV) at 900 compared to 600 °C. Also, the elemental and EDS investigation of MBOB established a broad diminution in O₂ and H₂ at 900 than 600 °C. The purest form of carbon with enhanced thermal stability, higher carbon content, smoothness, and bigger particles of biocarbon (verified by SEM) is accomplished at 900 °C. The electrical and thermal conductivity (EC and TC) of MBOB increased with increasing the temperature from 600 to 900 °C due to the close contact of biocarbon particles. Finally, an investigation of the particle size of MBOB established that the majority of particles are within 1.5 to 1.7 μm.

Keywords Slow pyrolysis · Mixed bio-oil · Biocarbon · Raman exploration · SEM · Particle size · Graphitic carbon

Highlights

- Waste mixed bio-oil was transformed into value-added bio-carbon.
- Temperature of pyrolysis played a primary role in the variation of bio-carbon yield and properties.
- Raman analysis of biocarbon showed enhanced graphitic content of the resulting bio-carbon.
- The purest form of carbon was obtained with greater thermal stability at 900 °C.
- Electrical and thermal conductivity of biocarbon increased with an increasing pyrolysis temperature.

✉ Manjusri Misra
mmisra@uoguelph.ca

✉ Amar K. Mohanty
mohanty@uoguelph.ca

¹ Bioproducts Discovery and Development Centre,
Department of Plant Agriculture, Crop Science Building,
University of Guelph, Guelph, ON N1G 2W1, Canada

² School of Engineering, Thornbrough Building, University
of Guelph, Guelph, ON N1G 2W1, Canada

Nomenclature

MBO	Mixed bio-oil
HHV	Higher Heating value
SEM	Scanning Electron Microscope
TGA	Thermogravimetric analyzer
EDS	Energy-Dispersive Spectroscopy
FTIR	Fourier-Transform Infrared Spectroscopy
MBOB	Mixed bio-oil-derived biocarbon
TC	Thermal conductivity
EC	Electrical conductivity
TD	Thermal diffusivity
SH	Specific heat analysis
TGA-FTIR	Thermogravimetric analyzer-Fourier-trans- form infrared spectroscopy
MDB	Miscanthus-derived bio-oil
ACSB	Areca catechu sawdust-derived bio-oil
MDBB	Miscanthus bio-oil-derived biocarbon
ACSBB	Areca catechu sawdust bio-oil-derived biocarbon
BET	Brunauer–Emmett–Teller

1 Introduction

The rapid growth of the earth's population, a growing shortage of energy resources, and the impacts of global warming have increased the necessity for clean energy generation, with the added impetus of effective waste management and reduction in emissions of greenhouse gases (GHG) [1, 2]. Over the last few decades, it has been established beyond doubt that fossil fuels, the primary source of energy, fall short of being both clean and sustainable [3]. Moreover, the consumption of fossil fuels for the generation of energy or in the transportation sector adds substantially to GHGs emissions. Against this backdrop, bio-oil has the potential to diminish the reliance on petroleum-based products. Bio-oil can be formed from the heating of materials in a non-oxidizing environment within 400–700 °C [4]. The core route for bio-oil generation from waste materials dovetails the pyrolysis process, where the liquid product yield from dry feedstocks is exploited via thermal disintegration of organic constituents in the non-appearance of oxygen. Thus, for the generation of bio-oil, which is a carbon-rich liquid, pyrolysis is a convenient technique [5]. Yet, among all the thermochemical technologies, pyrolysis was deemed an evolving technology for converting dry feedstocks into liquid (bio-oil), solid (biocarbon), and gaseous forms of energy within the stated time [4]. Pyrolysis has gained widespread acknowledgement for its multifaceted products and its innate capacity to generate the solid, liquid, and gaseous forms of energy in parallel [3]. However, the yield and the properties of final pyrolysis products vary with pyrolysis operating conditions and types of feedstocks [4]. In addition, the advanced application of bio-oil as a promising candidate was considered premature as substantial research was in progress [6]. In general, CO and CO₂ are the products of the gaseous phase, and in the liquid phase, a dark liquid presages bio-oil formation from the condensation of hot volatiles [4]. The bio-oil thus produced could be consumed either as a transportation fuel or employed in the boiler and furnace to create heat and power [7]. But the greater viscosity and moisture content, low calorific value and acidity, highly corrosiveness, and high instability in comparison with petroleum-based fuels circumscribe the direct application of bio-oil as a fuel in an engine [6, 8]. The fact that bio-oil is generally enriched with hydrocarbons, aromatics, acids, esters, phenols, furans derivatives, alkanes, ketones, ethers, amide, and aldehydes [9, 10] allows for the production of value-added chemicals such as resins, fertilizers, food flavoring, and making of soap [11].

Finally, the solid residue (biocarbon) can play an enormous role in meeting the energy demand in the form of heat and marks an inflection point in the real-world

demand to diminish global warming by arresting and saving atmospheric carbon [12]. It is well documented that the major portion of biocarbon formed by pyrolysis of biomass has a lower O/C and H/C ratio (0.1 to 0.3, respectively) caused by a boost in carbon content and a reduction in H₂ and O₂ [5]. This is possibly the root cause of dehydration reactions, breakdown of the oxygenated bonds, and the evaporation of lower molecular weight by-products aided by the lower H₂ and O₂ [13]. Biocarbon distribution in pyrolysis differs typically between 15 and 52 wt.%, subject to the operating conditions, the composition of the feedstock, and pyrolysis types [14]. The solid material formed from the slow pyrolysis of organic feedstocks has been strongly advocated for numerous technological applications such as bio-sensors, catalysts, energy storage and conversion devices [15], CO₂ capturing, catalysts, bio-adsorbents, fuel cells, supercapacitors, nanotubes, and medical applications [16]; fertilizers [17], and bio-composite materials [18]. The characteristics of biocarbon are dependent on the biochemical configuration of feedstocks and operating conditions such as temperature, residence time, heating rate, and particle size [4]. Among all the operating conditions, the rate of heating, size of particles, and temperature impacted the yield and properties of biocarbon substantially [4]. The sequestration of atmospheric carbon has become critical in combating the rapid change in the global climate. Since increased pyrolysis is part of the strategy to arrest the atmospheric carbon load, the resultant increased production of biocarbon and biochar suggests an upsurge in that bio-oil and syngas production is achievable [19]. As a natural corollary, it is critical to examine the transformation of pyrolysis by-products, like bio-oil conversion into valued biocarbon using slow pyrolysis, that lifts carbon sequestration, without the added risk of unsuitable dumping and expensive storage of bio-oil.

The present study explores the onversion of mixed bio-oil (MBO) into valued biocarbon using slow pyrolysis technique. Though the utilization of biocarbon touched a new height within a short time, the generation of biocarbon from biomass through slow pyrolysis grew extensively. To the best understanding of the author and from the literature surveyed, the biocarbon produced from MBO using the slow pyrolysis technique has not yet been explored. Therefore, the present study explores the slow pyrolysis of MBO to produce biocarbon from a hitherto unexplored source. Lastly, the features of the biocarbon formed at different temperatures were studied with various characterization devices (TGA, FTIR, SEM, Raman spectroscopy, EDS, and CHNS analyzer). The online characterization of hot gases against the temperature is also explored using TGA-FTIR under an inert ambiance.

2 Material and methods

2.1 Sample collection and preparations

MBO was received from the Bioproducts Discovery and Development Centre (BDDC) laboratory, Canada, gained from the slow pyrolysis of various biomass at different temperatures (450–900 °C). The MBO was collected from biomass such as pine nuts, peanuts shells, wheat straw, soya hulls, corn stover, spent coffee ground, chicken feather, coffee chaff, miscanthus, etc. MBO was placed in a separating funnel for 24 h for phase separation. The MBO was separated into two layers where the topmost layer is acknowledged as bio-oil (organic phase); however, the bottom-most phase is acknowledged as the aqueous phase (17–30 wt.%). The organic phase of the bio-oil is used in this study to produce the biocarbon.

2.2 Characterization of bio-oil and biocarbon

2.2.1 Elemental analysis, ash content analysis of biocarbon and bio-oil

Elemental analysis (carbon, hydrogen, nitrogen, and sulfur) is the primary step in evaluating the feasibility study of feedstocks. Elemental analysis of MBO and MBOB was calculated with an elemental analyzer (FLASH 2000, Thermo Fisher Scientific Inc., USA). The amount of oxygen was calculated by 100-(sum of C, H, N, and S). Further, inorganic residue (ash content) of MBO and MBOB was achieved through the ASTM D1762-84 in a Thermogravimetric analyzer (Q500, TA-Instrument, New Castle, Delaware, USA), while the acidity of the bio-oil was determined using a pH meter (Eutech waterproof, pH Spear). Further, HHV of MBO and MBOB was calculated using the equation below [20].

$$\text{HHV (MJ/kg)} = 32.7934 + 0.5321C^2 - 0.5321C - 2.8769H + 0.608CH - 0.2401N \quad (1)$$

where C = Carbon, H = Hydrogen, and N = nitrogen.

2.2.2 Thermal stability analysis of MBO and MBOB

The thermal stability profile of MBO and MBOB was analyzed in a TGA (Q500, TA-Instrument, New Castle, Delaware, USA) under an inert environment. The heating of the sample (8 mg) started from a temperature of 30–900 °C after placing the chosen sample in a platinum pan at a 10 °C min⁻¹ heating rate, whereas the flow of nitrogen gas was kept steady (50 mL min⁻¹) at all the time during the test.

2.2.3 TGA-FTIR analysis of bio-oil

TGA-FTIR study of MBO was accomplished in a TGA (Q5500, TA Instruments, USA) accompanied with FTIR (Nicolet 6700 FTIR spectrometer, Thermo-Scientific, USA). The organic phase of the MBO (7 mg) was placed in a crucible and heated from 30 to 900 °C at 20 °C min⁻¹ heating rate, while nitrogen flow rate was held steady (50 mL min⁻¹) throughout the experiment. After completing the experiment, Gram-Schmidt software was applied to identify the relative absorbance of the individual volatiles.

2.2.4 FTIR analysis of bio-oil and biocarbon

The identification of the functional groups present in the mixed bio-oil (MBO) and biocarbon (MBOB) was accomplished using FTIR-ATR (Nicolet 6700, Thermo-Scientific, USA). A small amount of sample was placed on the Attenuated total reflectance (ATR crystal), whereas the scanning started at a rate of 64 with the resolution of 4 cm⁻¹ in the range of 400–4000 cm⁻¹ wavenumbers.

2.3 Pyrolysis experiment

The generation of biocarbon (MBOB) from the slow pyrolysis of mixed bio-oil (MBO) was achieved from the horizontal tube pyrolyzer (Carbolite 1200 °C G-range). The outer surface of the tube furnace was manufactured with stainless steel, whereas inside the furnace, ceramic bricks were used. The reactor was manufactured with quartz glass in a cylindrical shape. The pyrolysis reactors mainly include a thermocouple, control panel, quartz reactor, ceramics boat, ceramic stoppers, gas rotameter, nitrogen cylinder, and conical flask. The control panel is used to regulate the desired temperature, heating rate, and residence time; however, the thermocouple is directly linked to the furnace that measures the accurate temperature inside the reactor. A ceramic boat was introduced to load the MBO that is positioned inside the quartz tube; however, the quartz tube is placed horizontally inside the electrical furnace. The gas rotameter is introduced to measure the nitrogen gas flow rate accurately throughout the experiment. The nitrogen gas was allowed to flow at a constant rate of 1.5 standard liters per minute (SLPM) throughout the test; however, gas was started 15 min earlier, allowing the test to vacate the undesirable impurities from the reactor. The stopper was used at both the ends of the quartz reactor to provide a balanced flow of the gases. MBO (10.0 ± 0.1 g) was engaged in the ceramic boat, and the pyrolysis test was performed at 600 and 900 °C, 10 °C min⁻¹ heating, and 30 min holding time. The holding time is a required time in which the experiment conquers the equilibrium. Furthermore, to certify the precision of biocarbon yield, the pyrolysis test was done twice. After the

accomplishment of the experiment, the reactor was allowed to be cooled up to 30 °C. Afterward, the solid residue that remained after the experiment was collected and kept in an airtight glass container. The yield of solid residue (biocarbon) was calculated using Eq. (2). The collected and dried biocarbon was then ball milled for 4 h using a Retsch ball mill machine at 200 rpm and again stored in an airtight glass container to stop moisture absorption. A complete layout of the experimental setup is shown in Fig. 1.

$$\% \text{ Yield of biocarbon} = \left[\frac{\text{Solid material left after the pyrolysis}}{\text{Weight of feeded biooil}} \right] \times 100 \quad (2)$$

2.4 Raman analysis

The amount of graphitic content in MBOB was conducted in a DXR2 Raman Spectroscopy (Thermo Scientific, USA). Each Raman spectra were analyzed with a 785 nm laser at 200 mW power. To analyze the accuracy and better quality of data, the Raman machine was functioned at 10 times zoom over a 50- μm slit. The exported excel data format from the Raman study was then fed into Origin lab software to identify the biocarbon graphitic content using two peaks fitting. The two peak fitting of biocarbon produced a correction coefficient (R^2) value greater than 0.95 in each instance; therefore, two peak fitting is preferred.

2.5 BET surface area and bulk density of biocarbon

Brunauer–Emmett–Teller (BET) surface area of the resulting biocarbon (MBOB) was measured with the Autosorb-iQ (Quantachrome Instruments) with ASiQwin 5 software. The biocarbon was first degasified at 150 °C for 180 min to

remove the moisture impurities in the sample. Further, an adsorption/desorption method was performed with multi-point BET as per ASTM standard D6556-19. The bulk density (BD) of MBOB was accomplished with the help of a digital balance and a measuring cylinder. The digital balance was introduced to measure the mass of the biocarbon, while the cylinder was used to compute the volume.

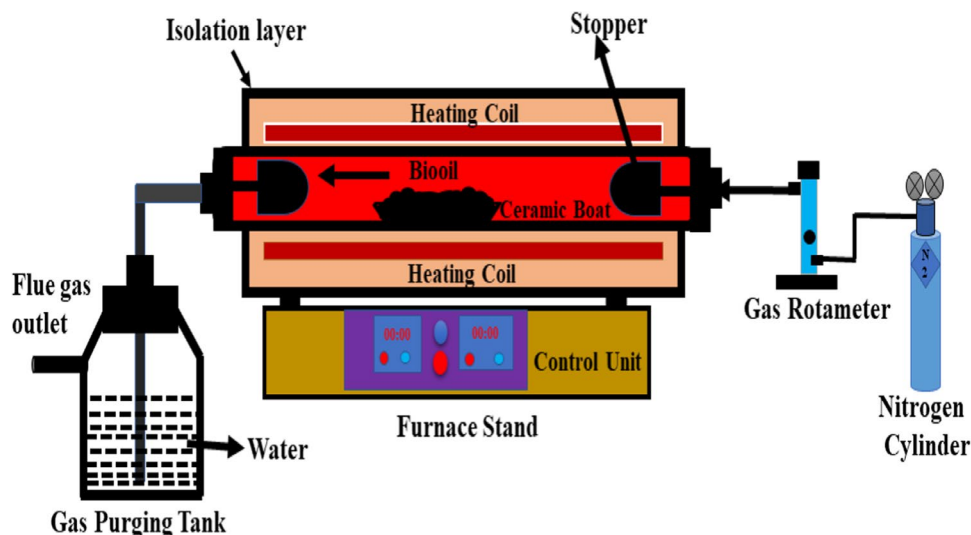
2.6 Electrical conductivity (EC), Thermal conductivity (TC), and Specific heat (SH) analysis of bio-carbon

The EC of MBOB was carried out with an Autolab PGSTAT302N, Netherlands. The 4-h ball-milled biocarbon was used to measure electrical conductivity. The required amount of biocarbon was filled in a clear hollow cylinder having a 10-mm internal diameter. For compacting the biocarbon, a piston of 1 kg was kept on the top of the cylinder and legalized for 30–40 s without pressing. One end of the electrode device was linked with the piston, and the other end was connected to the machine. Further, the thermal conductivity, diffusivity, and specific heat of MBOB were acquired with ThermTest Hot Disk TPS 500 Thermal Constants Analyzer. The 4-h ball-milled powder sample was placed on the measuring device where heating power, frequency time, and the radius of the used sensor were nominated as 120 mW, 60 Hz, 80 s, and 6 mm, respectively.

2.7 Scanning Electron Microscopy/ Energy-Dispersive Spectroscopy (SEM–EDS) and Particle Size Analysis of Biocarbon

The surface morphology and particle size examination of MBOB at 600 and 900 °C were carried out in an SEM

Fig. 1 Schematic arrangement of the pyrolysis-experimental setup



(SEM, Phenom ProXelectron microscope scanner, Phenom-World BV, Eindhoven, Netherlands) interconnected with EDS. SEM investigation of biocarbon was finished without surface coating. SEM image was acquired at 15 kV accelerating voltage without coating the biocarbon. EDS was hired to evaluate the elemental analysis (carbon and oxygen) of biocarbon at 15 kV with an acquiring time of 90 s. For the particle size examination, a maximum of four images were captured with fluctuating magnification to arrest varying sizes of particles, and the average value was testified. The biocarbon particle size was measured with a particle size analyzer (version 1.0.346.44124, Phenom-World BV, Eindhoven, Netherlands) to arrest the shape and particle size of an individual image. However, the recorded image was usually maintained with greater than 1000 particles for accurate data.

3 Results and Discussion

3.1 Physicochemical characterization of mixed bio-oil (MBO)

The elemental investigation of MBO is displayed in Table 1. The physicochemical properties of MBO are compared with miscanthus-derived bio-oil (MDB) [21] and areca catechu sawdust-derived bio-oil (ACSB) [22]. The ultimate analysis of MBO confirmed higher carbon content (70.40%) than MDB (43.60%) and ACSB (65.12%). The difference in the carbon percentage among the bio-oils was mainly due to the quality of bio-oil and its compositional dissimilarity. MBO and ACSB were produced in the laboratory, whereas the MDB was produced industrially; thus, the possibility of some impurities during MDB collection could not be ruled out. However, MDB and ACSB exhibit differences in carbon percentage due to the pyrolysis operating conditions and pyrolyzed feedstocks [4]. Further, the nitrogen content

in MBO was found to be higher (1.60%) than MDB (0.80%) due to a possibly compositional difference in feedstocks. The fact that MBO is derived from different biomass may be responsible for the higher nitrogen content. Moreover, the nitrogen content of ACSB is higher (2.43%) than that of MBO (1.60%) because of the existence of lignin content (~14%) in areca catechu sawdust which favors the formation of nitrogen during pyrolysis [22]. The hydrogen and oxygen content of MBO was found to be 5.60% and 21.80%, which was very close to the values for MDB and ACSB (Table 1). The lowered flame temperature of bio-oil with higher oxygen content reduced its utility as a fuel [23]. Finally, the sulfur content (0.56%) was found to be lower in MBO than in ACSB, indicating the formation of SO_x would be lower during pyrolysis and minimized the chances of corrosion in pipes and storage vessels [24]. The HHV of MBO at 28.55 MJ kg⁻¹ is well matched with ACSB and bio-oil derived from *cascabela thevetia* seeds [25]. The HHV of MBO demonstrated that it could be used for direct burning in the boiler and furnace to create heat and power [22]. The acidity (pH) of the MBO was alkali in nature (8.2), enhancing the HHV of bio-oil by reduction of proton ions [23]. In addition, the lower proportion of proton ions in bio-oil reduced the generation of water molecules during pyrolysis [23]. Finally, the ash content examination of MBO was found to be (0.95%), which is very close to ACSB (0.46%) but found to be lower than MDB (4.65%). The MDB was derived from the industrial facility; thus, there is a probability that some inorganic residue was added, which ultimately increased the ash content [21].

3.2 Thermal stability study of MBO

The thermal stability profile of MBO is displayed in Fig. 2. MBO decomposed into three significant zones recognized as a drying zone, an active pyrolytic zone, and finally, the char formation zone. The initial zone of the MBO confirmed mainly evaporation of water/moisture (dehydration zone) and some hot volatile products up to 100 °C. However, maximum degradation occurred in the second zone; therefore, it is recognized as a maximum decay zone. The bio-oil is a miscellaneous combination of several products that renders it multifaceted in nature. Most interestingly, the composition of bio-oil possibly changed with the types of biomass and its biochemical composition [26]. Bio-oil is formed from the degradation of cellulose, hemicellulose, and lignin; thus, the composition of bio-oil is subject to many variations. The breakdown of hemicellulose and cellulose typically produced aromatic and aliphatic hydrocarbons, acids, ketonic products, cycloalkane, furanic products, and mixed hydrocarbon [27], whereas the breakdown of lignin typically produced guaiacyl, p-hydroxyphenyl, syringyl, aromatic hydrocarbons, and various other hydrocarbons [28]. From Fig. 2, it was deceptive

Table 1 Physicochemical characterization of MBO and compared with MDB and ACSB

Analysis	MBO	MDB [21]	#ACSB [22]
C (%)	70.40 ± 0.18	43.6 ± 0.65	65.12 ± 0.20
H (%)	5.60 ± 0.89	6.1 ± 0.03	7.12 ± 0.10
O (%)	21.86 ± 1.01	21.6 ± 1.07	25.14 ± 0.8
N (%)	1.60 ± 0.05	0.8 ± 0.01	2.43 ± 0.14
S (%)	0.56 ± 0.005	0	0.92 ± 0.01
HHV (MJ/kg)	28.55 ± 0.12	-	28.38 ± 1.12
Acidity (pH)	8.20 ± 1.10	-	2.87 ± 0.10
Ash content (wt.%)	0.95 ± 0.042	4.65 ± 0.083	0.46 ± 0.014

*MDB = Miscanthus-derived bio-oil, ACSB = Areca catechu sawdust-derived bio-oil, MBO = Mixed bio-oil, HHV = Higher heating value

#Areca catechu sawdust-derived bio-oil was found at 500 °C and 80 °C min⁻¹ heating rate

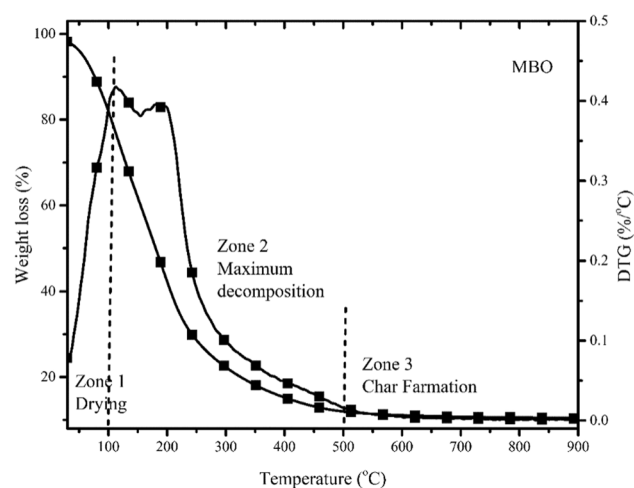


Fig. 2 Thermal stability analysis of MBO at $10\text{ }^{\circ}\text{C min}^{-1}$ heating rate

that the mass loss rate of MBO culminated at $114\text{ }^{\circ}\text{C}$ and $193\text{ }^{\circ}\text{C}$. A similar testified value was also reported by various authors [21, 29], confirming that the mixture of miscellaneous compounds decomposed at varied temperatures. TG profile of MBO also proved to have a minimal effect on the mass loss profile beyond $500\text{ }^{\circ}\text{C}$. Most of the compounds present in bio-oil (alkanes, phenols, and oxygenated products) are fragmented before $500\text{ }^{\circ}\text{C}$; only very few compounds decay beyond $500\text{ }^{\circ}\text{C}$; the latter is associated with lignin derivatives that actually turn into biocarbon [21]. DTG thermograph of MBO proved that maximum fragmentation rose in a wide temperature range from $100\text{--}500\text{ }^{\circ}\text{C}$, whereas the extreme fragmentation peaks were found at $114\text{ }^{\circ}\text{C}$ and $193\text{ }^{\circ}\text{C}$. The broad decomposition peak of MBO is accredited to low and heavy volatile products, like light aromatics and smaller molecular weight organic acids [21]. The boiling point of most of the compounds originates in the bio-oil altered from $150\text{--}270\text{ }^{\circ}\text{C}$, comprising phenol ($182\text{ }^{\circ}\text{C}$), cresol ($200\text{ }^{\circ}\text{C}$), guaiacol ($205\text{ }^{\circ}\text{C}$), catechol ($246\text{ }^{\circ}\text{C}$), syringol ($261\text{ }^{\circ}\text{C}$), and isoeugenol ($267\text{ }^{\circ}\text{C}$) [21]. It was also established that bio-oil produced from the slow pyrolysis contains $\sim 10\text{--}15\text{ wt.}\%$ of organic acids (propionic acid, hexadecenoic acid, acetic acid, and formic acid) [6, 30]. The fragmentation of bio-oil within $100\text{--}140\text{ }^{\circ}\text{C}$ mainly showed acetic acids ($118\text{ }^{\circ}\text{C}$), formic acid ($101\text{ }^{\circ}\text{C}$), and propionic acid ($141\text{ }^{\circ}\text{C}$) [21]. Additionally, benzene and toluene were also fragmented within $100\text{--}140\text{ }^{\circ}\text{C}$ [21]. Furthermore, bio-oil that decomposed in the range of $400\text{--}500\text{ }^{\circ}\text{C}$ and beyond $500\text{ }^{\circ}\text{C}$ primarily exhibited disintegration of lignin-based oligomeric products [31].

3.3 TGA-FTIR analysis of MBO

TGA-FTIR is an investigative technique that records the hot volatiles formed during the pyrolysis of the input materials against time or temperature. Moreover, the data recorded

from the pyrolysis of feedstocks in TGA-FTIR can be applied to evaluate numerous environmental effects [32]. TGA-FTIR is also able to quantify the composition of products formed from hot volatiles. The 3D surface plot of MBO formed from the TGA-FTIR is shown in Fig. 3a, and the relative quantity of hot volatiles formed from the heating of feedstock is presented in Fig. 3b. From the 3D surface plot of MBO, it is clear that most of the hot volatiles escaped between 12 and 44 min. The peak-by-peak analysis of MBO confirmed that peaks 3673 cm^{-1} ascribed the existence of water and alcohol in the bio-oil. The biomass pyrolysis formed a substantial quantity of water by reacting an oxygen molecule with hydrogen. Further, the band peak 2930 cm^{-1} established the release of hydrocarbons [33], whereas peak 1769 cm^{-1} established the announcement of carbonyl products in the MBO. The peak at 2366 cm^{-1} accredited to the asymmetric vibrations established the persistent presence of CO_2 [34]. The peaks 1114 and 1130 cm^{-1} related to C-O stretching proved the presence of ethers [34].

The quantity of hot volatiles released at the time of pyrolysis of MBO is shown in Fig. 3b; where ethers were the highest constituents (30.95%), followed by hydrocarbons (24.54%), carbonyl (20.65%), carbon dioxide (10.75%), water/alcohol (10.65%), and finally carbon dioxide (2.42%). MBO was derived from different temperatures and feedstocks, which contributed to a higher amount of oxygenated compounds during pyrolysis. Although the aqueous phase was separated with a separating funnel, the remanent oxygenated compounds present in the bio-oil created a higher percentage of ethers. The type of pyrolysis (slow and fast) and the operating conditions substantially alter the properties of the product [4, 35]; probably, bio-oil obtained at lower pyrolysis temperature results in a higher quantity of oxygenated products. Hydrocarbons rank first in the amount of hot volatiles released from MBO. It is well documented that biomass pyrolysis yields around 30–42% hydrocarbons [6, 30]. Further, the carbonyl compounds were ranked second in the amount released during pyrolysis of MBO by oxidation of unsaturated fatty acids (carboxylic acid with a long aliphatic chain, which is either saturated or unsaturated), resulting in a variety of secondary products such as aldehydes, carboxylic acids and ketones [36]. Carbon dioxide was found to be 10.75% during pyrolysis of MBO by the formation of the decarboxylation reaction. Decarboxylation reaction favours the formation of CO_2 by abolishing a carbon atom from a chain of carbon [3]. The amount of carbon monoxide was 2.42%, probably due to the decarbonylation reaction [3]. Decarbonylation is an organic route that favours the exclusion of CO by substituting a carbon atom from the chain of carbons [3]. Finally, the water or alcohol was 10.65% during pyrolysis of MBO stimulated by the generation of dehydration reaction [3]. Overall, the pyrolysis of MBO

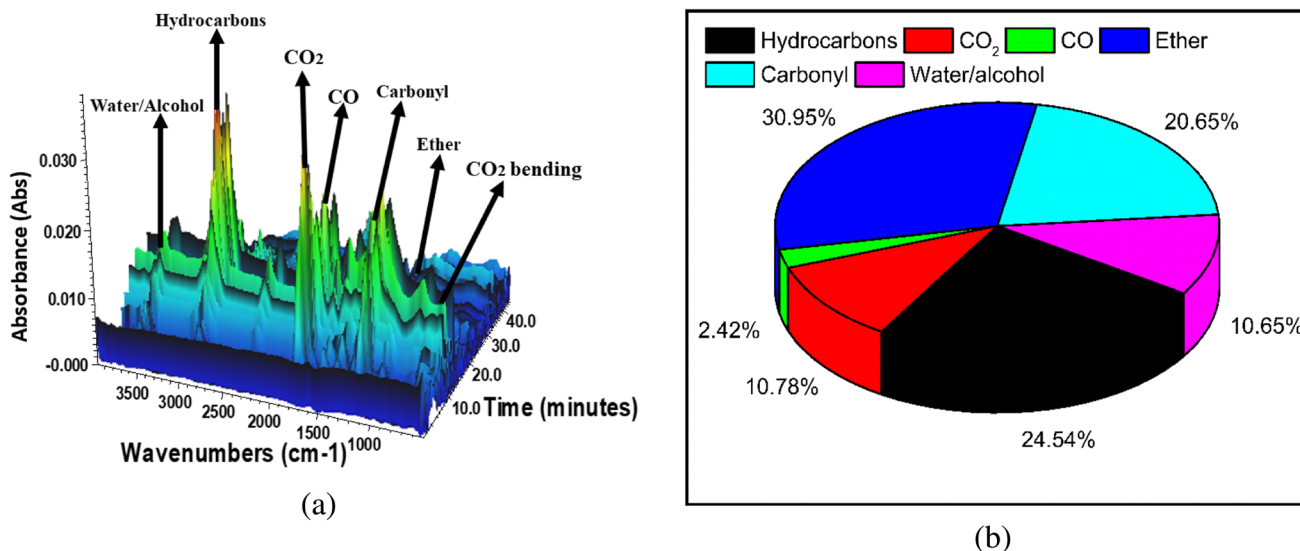


Fig. 3 TGA FTIR analysis of (a) 3D plot of MBO and (b) hot volatile released during pyrolysis of MBO

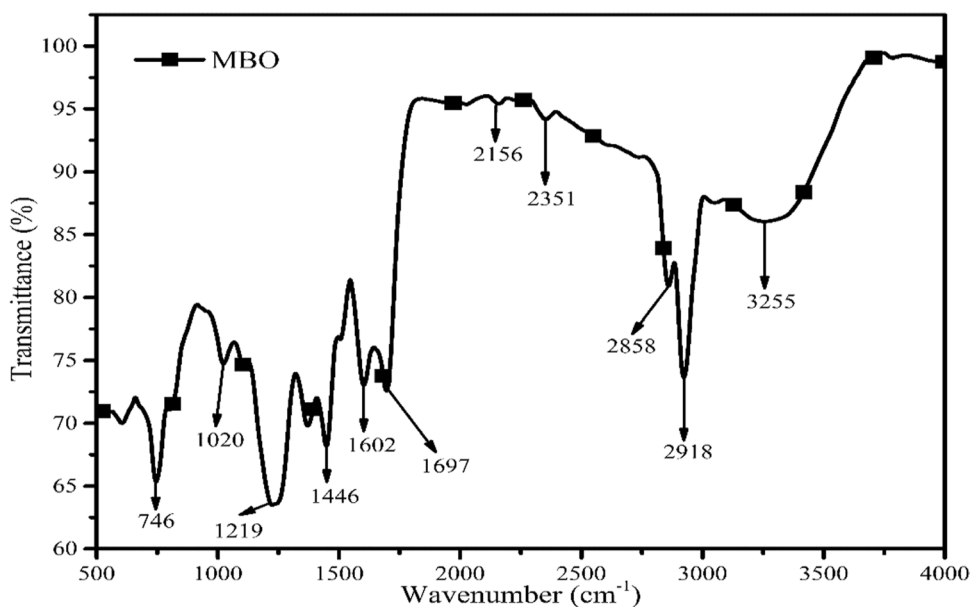
exhibited the highest release of ethers, hydrocarbons, and carbonyl products.

3.4 FTIR analysis of MBO

FTIR spectra recorded between wavenumber against transmittance are displayed in Fig. 4. The band peak 3255 cm^{-1} credited to -OH stretching vibration is attributed to the presence of water, alcohol, and aromatics [37]. The water, alcohol, and aromatics admixture in water are reflected in the FTIR analysis. The band peaks 2918 and 2858 cm^{-1} are accredited to the aliphatic C-H stretching vibration, while peak 2156 cm^{-1} represented C-C stretching vibrations, and

peak 1456 cm^{-1} allied with C-H bending vibration established the incidence of alkanes and aromatics [21, 38]. The degradation of hemicellulose and cellulose against temperature mainly yielded hydrocarbon and some aromatics, a clear validation of the abundance of these compounds in bio-oil [39]. The band peak 1219 cm^{-1} ascribed to C-O stretching vibration was credited to the existence of phenol and alcohol [21]. Further, band peaks 1602 cm^{-1} and 1697 cm^{-1} displayed C=O stretching vibration that designates the incidence of acid (carboxylic acid), ketones, aldehyde, and esters [21]. The biomass decomposed at a lower temperature ($\sim 400\text{--}450\text{ }^\circ\text{C}$) usually formed acids, alcohol, water, and other oxygenated products [40]. The peak at 1050 cm^{-1} is

Fig. 4 FTIR spectrum of MBO



recognized as the stretching of C-O that indicates an attendance of alcohol and aliphatic ethers [41]. The peaks originating within 500–900 cm^{-1} represented an aromatic C-H stretching vibration that exhibited attendance of poly and mono aromatic in the bio-oil [21]. Overall, FTIR examination of MBO established the attendance of phenols, aromatic, alcohol, acids, ketones, esters, and aldehyde, which also have good agreement with other stated literature [21].

3.5 Physicochemical Characterization of MBOB

The physical and chemical properties of mixed bio-oil-derived biocarbon (MBOB) at 600 and 900 °C are itemized in Table 2 and matched with miscanthus bio-oil-derived biocarbon (MDBB) [21]. The yield of biocarbon at 600 and 900 °C was noticed to be 13.47% and 10.27%, respectively. It was noted that by boosting the temperature from 600 to 900 °C, the biocarbon yield declined by around 3.2% due to complete pyrolysis. The term complete pyrolysis denotes the removal of all impurities from the biocarbon. Titiladunayo et al. (2012) pyrolyzed a variety of biomass at 400, 500, 600, 700, and 800 °C in a fixed-bed reactor and stated that with an upsurge in temperature from 400 to 800 °C, the biocarbon yield declined from 37 to 29%, by removal of all contamination from the biocarbon [42]. Similar results were found for the pyrolysis of MDBB at 600 and 900 °C with 30 and 60 min residence time [21]. This showed that lower pyrolysis temperature produced a higher yield of biocarbon; however, higher temperature produced a lower yield but an acceptable quality of biocarbon. Most obviously, the higher yield of biocarbon is connected to the inferior carbon purity due to undigested impurities in the biocarbon. Also, MBOB gives the lowest yield of biocarbon by virtue of the compositional difference in the bio-oil compared to MDBB. The bio-oil employed in MBOB was found to be purer than the

bio-oils used in MDB, thus making purer biocarbon possible in MBOB. Additionally, the operating temperature of pyrolysis may be another possible reason for reduced biocarbon yield.

The ultimate study of MBOB proved that with boosting in temperature from 600 to 900 °C, the amount of carbon content enlarged by the elimination of oxygen and hydrogen molecules in the biocarbon (Table 2) [30]. At a higher temperature (900 °C), the maximized heat and mass exchange favored the generation of the primary dehydration reaction and consequently reduced the O_2 and H_2 molecules in the biocarbon [22]. The ultimate study of MBOB confirmed the attendance of higher carbon content (82.78 and 89.20% at 600 and 900 °C, respectively) than MDBB (76 and 80% for 600 and 900 °C, respectively). The higher carbon percentage arose from the dissimilarity in the composition of bio-oil and the pyrolysis conditions. A similar finding was also conveyed for the pyrolysis of MDB into biocarbon [21]. Most interestingly, it was detected that the biocarbon derived at a lower temperature (600 °C) has less carbon purity than higher temperatures (900 °C) as materials remained uncooked at lower temperature biocarbon. Further, the ultimate analysis of MBO revealed biocarbon contained higher nitrogen content (6.61 and 6.96% for 600 and 900 °C, respectively) than MDBB (1 and 0.70% for 600 and 900 °C, respectively) as deamination and cyclization reactions during pyrolysis [43]. There is also the possibility that some nitrogen molecules trapped in the biocarbon pores during the pyrolysis contribute to the higher nitrogen content in the bio-carbon. The hydrogen and oxygen content of MBOB matched well with MDBB at 600 and 900 °C (Table 2). The ash content study of MBOB proved that with an upsurge in temperature from 600 to 900 °C, the percentage of ash was augmented to around 0.40% due to the exclusion of undigested materials from the biocarbon. The HHV of MBOB

Table 2 Physicochemical characterization of biocarbon derived from slow pyrolysis of MBO and matched with MDBB

Parameters	MBOB		MDBB [21]	
	600	900	600	900
Yield (wt.%)	13.47 ± 0.31	10.27 ± 0.21	32.61 ± 0.19	30.05 ± 0.21
C (%)	82.78 ± 0.06	89.20 ± 0.02	80.00	76.00
H (%)	2.40 ± 0.04	1.62 ± 0.02	2.10	1.40
O (%)	8.30 ± .02	2.30 ± 0.01	6.00	4.00
N (%)	6.61 ± 0.02	6.96 ± 0.02	1.00	0.70
S (%)	-	-	-	-
H/C	0.347	0.218	0.314	0.221
O/C	0.075	0.019	0.056	0.039
HHV (MJ/kg)	37.47 ± 1.1	43.00 ± 0.80	-	-
BET Surface area (m^2/g)	1.02 ± 0.02	0.04 ± 0.06	-	-
Bulk density (kg/m^3)	425.12 ± 1.2	431.08 ± 1.2	-	-
Ash content (wt.%)	1.73 ± 0.05	2.13 ± 0.06	10.29 ± 1.95	13.88 ± 1.58

*MDBB = Miscanthus bio-oil-derived biocarbon, MBOB = Mixed bio-oil-derived biocarbon

was found to be 37.47 and 43.00 MJ kg⁻¹ at 600 and 900 °C, respectively. The alteration in HHV ascended by virtue of the improved elemental composition of biocarbon (C, H, N, and S). Furthermore, the bulk density (BD) of MBOB was 425.12 kg m⁻³ at 600 °C and 431.08 kg m⁻³ at 900 °C, respectively. BET surface area of MBOB was found to be 1.02 and 0.04 m² g⁻¹ at 600 and 900 °C, respectively, by the deletion of pores from the biocarbon (proven by SEM study). The difference in the composition of feedstocks and pyrolysis conditions contributes to the very different surface morphology of the MBOB, from bio-oils derived from lignocellulosic biomass.

3.6 EDS analysis of Biocarbon

The energy-dispersive spectroscopy (EDS) study of MBOB is listed in Table 3. The final exploration of MBOB exposed a considerable alteration in oxygen and hydrogen post-pyrolysis. EDS examination of MBOB showed that the oxygen is higher in MBOB than obtained by the results of the elemental analyzer (Tables 2 and 3). It was also established that the reduction of O₂ and H₂ was higher at 900 than 600 °C as a result of increased dehydration reactions [23]. Also, the temperature-dependent exclusion of O₂ and H₂ may be accredited to the splitting of weaker bonds inside the biocarbon [44]. The similar importance and outcome of temperature on the elemental composition of biocarbon were also attested by many studies [45, 46].

3.7 Thermal stability of MBOB

The thermal decomposition plot of MBOB at 600 and 900 °C is displayed in Fig. 5. The TG profile of MBOB displays that 900 °C biocarbon has higher thermal stability than 600 °C biocarbon. The biocarbon derived from the higher temperature (900 °C) had all the adulteration digested, whereas lower temperature biocarbon contained some undigested impurities such as hydrocarbons, which lowered the biocarbon thermal stability. Moreover, the TGA study revealed that biocarbon collected at 600 and 900 °C possessed thermal stability up to 150–170 °C with a weight loss of ~1.10 and 1.58%, respectively. Overall, the thermal decomposition profile of MBOB demonstrated around 15.43

and 8% at 600 and 900 °C within 30–900 °C. The 600 °C biocarbon decomposed at higher than 900 °C, mainly by the decay of undigested impurities in biocarbon [21]. DTG thermograph demonstrated that the highest mass loss peak at 600 °C was found at ~694 °C; however, 900 °C biocarbon did not spectacle any peaks of breakdown. TGA and DTG study of the present work showed good compatibility with the reported study of MDBB [21]. It is well acknowledged that pyrolysis of bio-oil favored the formation of C=C bond-based products, especially at higher temperatures and non-oxidizing conditions. It is well documented that the C=C

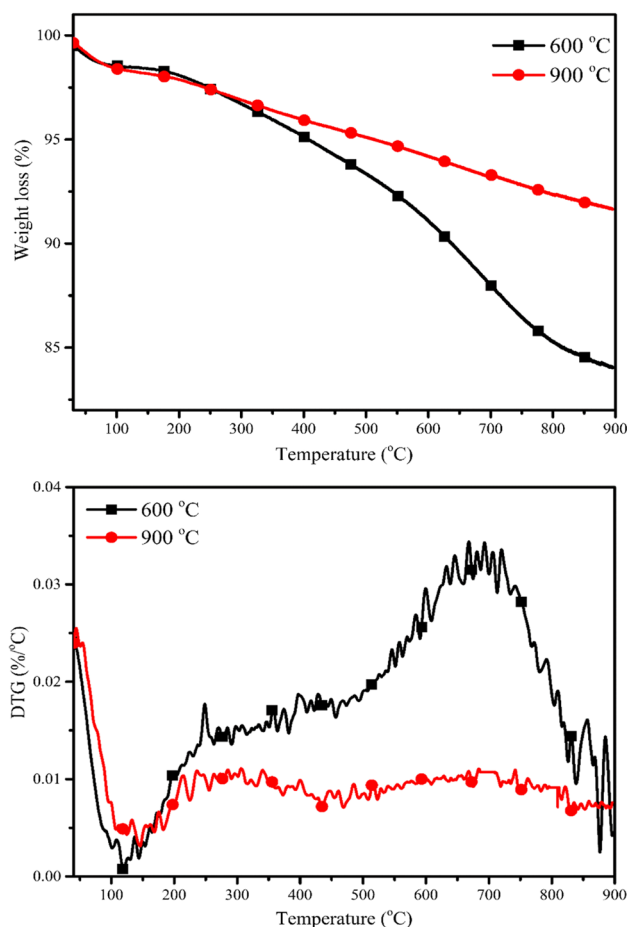


Fig. 5 TGA and DTG profile of MBOB at 600 and 900 °C

Table 3 EDX analysis of MBOB at 600 and 900 °C

Temperature (°C)	MBOB		MDBB [21]	
	Carbon (wt.%)	Oxygen (wt.%)	Carbon (wt.%)	Oxygen (wt.%)
600	79.8033 ± 0.246	20.1967 ± 0.246	82	18
900	85.0467 ± 0.219	14.9533 ± 0.219	86	14

* Miscanthus bio-oil-derived biocarbon was taken at 600 and 900 °C with 60 min residence time

bonds formed in the biocarbon are generally beyond 300 °C [21], whereas the accumulation of biocarbon happened after the exclusion of O₂ or its associated functional groups [47]. The higher temperatures (900 °C) result in the refined structure of carbon that can be verified in the SEM study of biocarbon. Similar conclusions of the breakdown of biocarbon gained at diverse temperatures are also reported on miscanthus [48] and MDB [21]. Overall, biocarbon formed at the higher temperature (900 °C) displayed a lower mass loss and maximal removal of contaminants with maximum purity of biocarbon.

3.8 FTIR study of MBOB

FTIR spectra drawn between wavenumber against transmittance are exhibited in Fig. 6. The FTIR spectra of MBOB are very different from the MBO because of the exclusion of the majority of functional groups through thermal treatment. The biocarbon derived at 600 °C displayed the attendance of band peak 1555 cm⁻¹ qualified to C-H bending vibration, showcasing the appearance of hydrocarbon and aromatics [21]. The band peak at 1146 cm⁻¹ recognized to C-O stretching vibration confirmed the attendance of phenols [21, 49]. The band peak 741 cm⁻¹ linked with C-H stretching vibration exhibited attendance of poly and mono aromatic in biocarbon [21]. Further, biocarbon gained at 900 °C displayed the band peak at 1521 cm⁻¹ and was ascribed to C-H bending vibration and signals the presence of alkanes [33]. Finally, the band peak at 2346 cm⁻¹ ascribed to C-C stretching vibrations mainly represents aromatics [21, 49].

3.9 Raman spectroscopy analysis of biocarbon

Raman spectroscopy is a spectroscopic tool typically employed to determine vibrational modes of molecules of

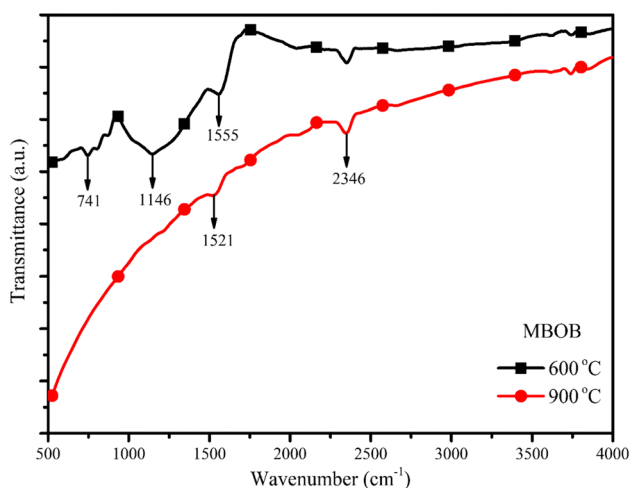


Fig. 6 FTIR spectra of MBOB biocarbon at 600 and 900 °C

the targeted material. Raman spectrum was plotted using wavenumber against the intensity in Fig. 7(a and b). Raman spectrum was inspected from 800 to 2000 cm⁻¹ to calculate the graphitization in biocarbon, with the I_D/I_G ratio accessible in Table 4. Two peaks were designated to analyze the graphitization content in biocarbon. The band peak D is designated in the range of 1354–1357 cm⁻¹, and band peak G is designated in the range of 1568–1575 cm⁻¹. Similar conclusions were also made for the chicken feather biocarbon [33]. As per the literature, the band peak D is accredited to sp² orbital and exhibited the disordered content; however, the band peak G is accredited to sp² orbital of the graphitic content. From the Raman study of MBOB, I_D/I_G ratio was found to be 0.8587 and 0.5805 for 600 and 900 °C, which is lower than the I_D/I_G ratio of chicken feather biocarbon (1.07 at 600 °C, respectively) [33]. The lower value of the ratio of I_D/I_G established the higher the graphitization of biocarbon [33, 50]. During Raman investigation, the peak

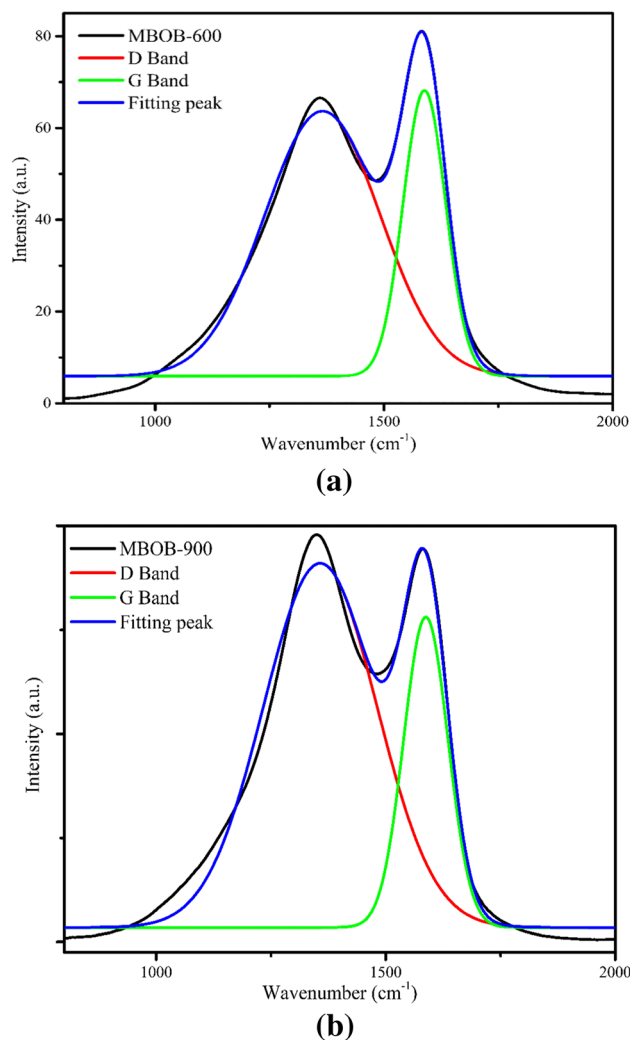


Fig. 7 Raman spectra of MBOB at (a) 600 °C and (b) 900 °C

Table 4 I_D/I_G ratio of MBOB gained at 600 and 900 °C

Temperature (°C)	I_D/I_G ratio
600	0.8557
900	0.8505

I_D associated with C–C bonds is recognized by the aromatic rings [51]. However, the peaks I_D designate that the relative strength is connected to the higher content of carbon in the biocarbon, as revealed by the Raman spectroscopy study of biocarbon [52]. Further, the peak I_G established the C=C bond ascribed to the relation with an aromatic structure, which is also sustained by FTIR of biocarbon [52].

3.10 Thermal conductivity (TC), Electrical conductivity (EC), Thermal diffusivity (TD), and Specific heat (SH) of biocarbon

Electrical conductivity (EC) of MBOB was carried out at 1 kg weight, and the obtained value is itemized in Table 5. The result indicates that the EC of biocarbon was expanded by boosting the temperature from 600 to 900 °C. The increased tendency of EC of biocarbon arose by the synergistic interaction between interparticle of biocarbon with boosting temperature from 600 to 900 °C, which allows the flowing of electricity [53]. In other words, the biocarbon particles interact with each other in such a way that the flow of electricity between biocarbon particles is improved, thus, expanding the EC of biocarbon. Hoffmann et al. (2018) studied the electrical conductivity of bio-based carbonaceous powder materials at dynamic temperatures of 600, 800, and 900 °C and concluded that the EC of biocarbon increased with an increase in temperature and pressure due to closer particle contact [54]. The average EC of MBOB was found to be 0.01011 S m⁻¹ and 0.38106 S m⁻¹ at 600 and 900 °C, respectively. The attained EC of MBOB at 900 °C matched well with carbon resulting from lignin (0.2 S m⁻¹) and black carbon (4.0 S m⁻¹) [55]. Moreover, the EC of MBOB gained at 600, and 900 °C is higher than the reported value of MDB (Table 5). However, the EC obtained at 600 °C is lower than elemental carbon derived from lignin and carbon blacks. It is

interesting to describe that the EC of elemental carbon derived from lignin and carbon blacks was obtained at a higher pressure than in the present study; therefore, they recorded a higher value of EC. The EC of the sample is extremely sensitive to operational pressures [56].

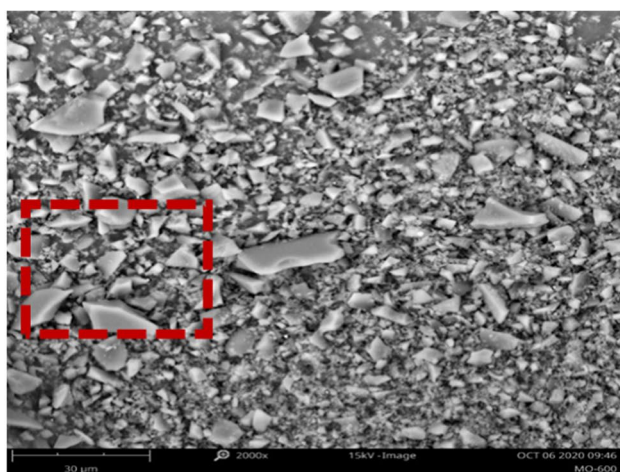
Thermal conductivity (TC), thermal diffusivity (TD), and specific heat (SH) of MBOB are documented in Table 5. It was proven that the TC of MBOB enlarged with an upsurge in temperature from 600 to 900 °C by bigger free electrons and lattice vibrations of carbon atom (higher phonon propagation); thus, in turn, increasing the TC of biocarbon [57]. The increased tendency of TC of biocarbon was also testified for MDBB [21]. The average thermal conductivity of MBOB was recorded at 0.12945 and 0.19798 W m⁻¹ K⁻¹ at 600 and 900 °C respectively. The calculated value of TC of MBOB is very adjacent to the amorphous carbon (0.01–2 W m⁻¹ K⁻¹) [58] and lignin-derived carbon [55]. Further, the thermal diffusivity (TD) of MBOB was found to be augmented by boosting the temperature from 600 to 900 °C through the close contact of the intraparticle of biocarbon. The average TD of MBOB was found to be 0.09701 and 0.16788 mm² s⁻¹ for 600 and 900 °C. Finally, the average specific heat of the MBOB was found 1.3674 and 1.1792 MJ m⁻³ K⁻¹ for 600 and 900 °C; however, the specific heat of the MBOB did not follow any trend.

3.11 SEM and particle size analysis of biocarbon

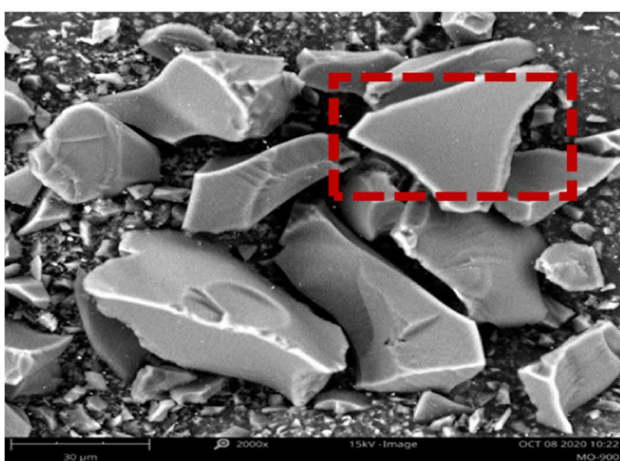
Scanning electron microscope (SEM) was employed to quantify the morphological appearances of MBOB at 600 and 900 °C; however, the recorded image at 2000× is presented in Fig. 8. The morphological presences of biocarbon became highly convoluted by the accumulation of different varieties of minerals. There are many chemical reactions such as dehydration (removal of moisture), decarbonylation (removal of CO), and decarboxylation (loss of carboxyl group) formed during pyrolysis, which transformed the biocarbon morphology [59]. From Fig. 8, SEM examination of MBOM revealed the usual surface design with lots of tiny pores caused principally by the discharge of countless hot volatiles during pyrolysis. Moreover, the structure and size of pores of biocarbon changed frequently with

Table 5 Thermal conductivity, electrical conductivity, Thermal diffusivity, and specific heat of MBOB at 600 and 900 °C

Temperature	Electrical conductivity (S m ⁻¹)	Thermal conductivity (W m ⁻¹ K ⁻¹)	Thermal diffusivity (mm ² s ⁻¹)	Specific heat (MJ m ⁻³ K ⁻¹)	References
600 °C	0.01011 ± 0.0008316	0.12945 ± 0.00508	0.09701 ± 0.0215	1.3674 ± 0.2228	Present Work
900 °C	0.38106 ± 0.0007866	0.19798 ± 0.0026	0.16788 ± 0.00514	1.1792 ± 0.0910	Present Work
Coal	-	0.26	0.15	1.70	[21]
MDB600	0.002761 ± 5.659E-06	-	-	-	[21]
MDB900	0.001489 ± 2.370E-05	-	-	-	[21]



(a)



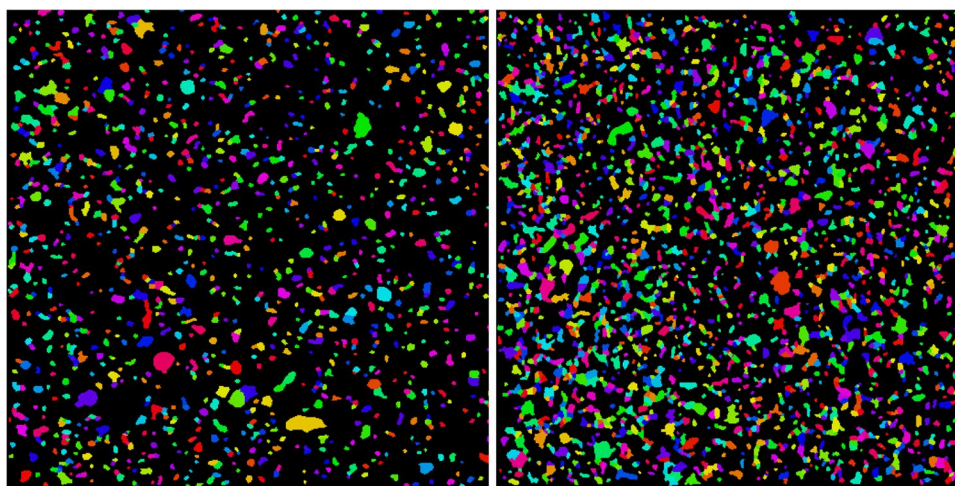
(b)

Fig. 8 Morphology analysis of MBOB (SEM) at (a) 600 and (b) 900 °C

changed pyrolysis conditions, with specific reference to the temperatures. SEM image revealed that biocarbon generated at 900 °C displayed very hard, smooth, and bigger particles than biocarbon from 600 °C. This modification may be attributed to the pyrolysis of bio-oil at a higher temperature, which yielded a refined and considerably more thermal stable carbon (TGA and FTIR results also supported this postulation). Additionally, interparticle interaction between the particles of carbon in the non-appearance of oxygen and hydrogen will enhance the shape and alignment of the carbon particles before and after squeezing.

The particle size study of the MBOB at 600 and 900 °C was explored with SEM connected with a particle size analyzer. The recorded image is shown in Fig. 9, whereas the calculated values are listed in Table 6. Due to the irregular shapes and sizes of biocarbon particles, the image analysis techniques such as SEM have been applied. However, the particle size of MBOB is studied at 4 h ball milling time. From Table 6, it is observed that lower temperature biocarbon (600 °C) was facile to smash into reduced particles due to less thermal stability, whereas higher-temperature biocarbon (900 °C) was hard to smash due to greater thermal stability. The average size of the particle originated to be 1.53 and 1.74 µm at 600 and 900 °C, respectively, whereas the median particle size of biocarbon was initiated to be 1.36 and 1.54 µm at 600 and 900 °C, respectively. Moreover, the maximum particle size was found to be 3.29 and 9.12 µm at 600 and 900 °C, respectively. Overall, between 600 and 900 °C, biocarbon gained at 600 °C gives the maximum amount of nano-carbon (<800 nm) by the smashing of larger particles into reduced particles than at higher temperature biocarbon (Table 6). Also, the extreme amount of particles is originated in the 1 µm range (<2 µm), followed by 2 µm (<3 µm) and <1 µm. Overall, the maximum amount of particles originated in 1 µm.

Fig. 9 SEM image of MBOB at (a) 600 °C, and (b) 900 °C



(a)

(b)

Table 6 Particle size analysis of MBOB at 600 and 900 °C

Temperature	Average particle size	Median Particle size	Aspect ratio	< 500 nm (%)	< 800 nm (%)	< 1µm (%)	< 2µm (%)	< 3 µm (%)	< 4 µm	< 5 µm	> 5 µm	Max. size particle detected (µm)
600	1.53 µm	1.36 µm	0.677	0.34	10.18	6.98	65.34	13.24	3.01	0.73	0.19	3.29 µm
900	1.74 µm	1.54 µm	0.700	0.025	3.55	4.45	66.38	18.53	5.1	1.42	0.58	9.12 µm

4 Conclusions

The produced biocarbon from bio-oil at 600 and 900 °C showed improved properties (carbon content, HHV, and surface morphology) than biomass-derived biocarbon. In this work, a slow pyrolysis technique was employed to recover the carbon by converting the MBO into valuable solid biocarbon. Although pyrolysis of bio-oil is still in the premature stage, the recuperation of valuable products (biocarbon) from the bio-oil has displayed waste bio-oil utilization. Overall, the produced biocarbon and its properties are strongly altered by the pyrolysis temperature. Further, an elemental examination of biocarbon established a substantial improvement in the C and H content with an upsurge in the temperature from 600 to 900 °C. Also, 900 °C biocarbon decomposed lower than 600 °C biocarbon by increased thermal stability. The functional group study showed an attendance of alkanes and aromatic compounds, while Raman exploration recognized a highly graphitic content in the high-temperature biocarbon. SEM examination also recognized that a higher temperature of biocarbon had enhanced the properties of (improved surface properties). The overall characterization of biocarbon from bio-oil showcased enhanced properties over biomass-derived biocarbon that can be employed for different industrial applications including supercapacitors, batteries, fuel-cells and composites.

Acknowledgements The authors would like to thank the following for their financial support to carry out this research: i) the Ontario Ministry of Agriculture, Food and Rural Affairs (OMAFRA), Canada/University of Guelph–Bioeconomy for Industrial Uses Research Program (Project Nos. 030331 and 030332); (ii) the Natural Sciences and Engineering Research Council (NSERC), Canada Discovery Grants (Project No. 401111); (iii) OMAFRA-Gryphon’s Leading to the Accelerated Adoption of Innovative Research (LAAIR) Program (Project No. 030416); iv) OMAFRA-Ontario Agri-Food Research Initiative (Project No. 055217); and v) the Ontario Ministry of Economic Development, Job Creation and Trade ORF-RE09-078 (Project Nos. 053970, 054345). Special thanks go to all the agencies for their donation of the samples. In this study, a) chicken feather was supplied by Maple Leaf foods Canada; b) Miscanthus was supplied by Prism Farms, 731 Mersea Road 6 Leamington, Ontario, Canada; c) corn stover and wheat straw were collected from the Salem Creek farms, 2408 Concession 4, Teeswater, Ontario, Canada; d) spent coffee ground was collected from the University of Guelph coffee stands; e) pine nuts were purchased from Nuts.com, Cranford, NJ, 07016, USA; f) coffee chap was supplied by Competitive Green Technologies, Leamington, Ontario, Canada; and g) peanut shells were donated by Picard Foods Partnership (Waterford, Ontario, Canada).

Author contribution All the authors have equal contribution to the present study.

Declarations

Conflicts of interests The authors declare that they have no known competing financial interest or person relationship that could have appeared to influence the study reported in the present study.

Open Access This article is licensed under a Creative Commons Attribution 4.0 International License, which permits use, sharing, adaptation, distribution and reproduction in any medium or format, as long as you give appropriate credit to the original author(s) and the source, provide a link to the Creative Commons licence, and indicate if changes were made. The images or other third party material in this article are included in the article's Creative Commons licence, unless indicated otherwise in a credit line to the material. If material is not included in the article's Creative Commons licence and your intended use is not permitted by statutory regulation or exceeds the permitted use, you will need to obtain permission directly from the copyright holder. To view a copy of this licence, visit <http://creativecommons.org/licenses/by/4.0/>.

References

- Wilson F, Tremain P, Moghtaderi B (2018) Characterization of biochars derived from pyrolysis of biomass and calcium oxide mixtures. *Energy Fuels* 32(4):4167–4177
- Mishra RK (2022) Pyrolysis of low-value waste switchgrass: Physicochemical characterization, kinetic investigation, and online characterization of hot pyrolysis vapours. *Bioresour Technol* 347:126720
- Mishra RK, Mohanty K, Wang X (2020) Pyrolysis kinetic behavior and Py-GC-MS analysis of waste dahlia flowers into renewable fuel and value-added chemicals. *Fuel* 260:116338
- Akhtar J, Amin NS (2012) A review on operating parameters for optimum liquid oil yield in biomass pyrolysis. *Renew Sustain Energy Rev* 16(7):5101–5109
- Hossain A, Davies P (2013) Pyrolysis liquids and gases as alternative fuels in internal combustion engines—A review. *Renew Sustain Energy Rev* 21:165–189
- Mohan D, Pittman CU Jr, Steele PH (2006) Pyrolysis of wood/biomass for bio-oil: a critical review. *Energy Fuels* 20(3):848–889
- Beran M, Axelsson L (2014) Application of pyrolysis oil in the OP16 gas turbine—development of a low calorific fuel combustor. *PyNe Newsl* 35:16–17
- Jacobson K, Maheria KC, Dalai AK (2013) Bio-oil valorization: a review. *Renew Sustain Energy Rev* 23:91–106
- Chen L et al (2015) Study on pyrolysis behaviors of non-woody lignins with TG-FTIR and Py-GC/MS. *J Anal Appl Pyrol* 113:499–507
- Mishra RK, Kumar V, Mohanty K (2020) Pyrolysis kinetics behaviour and thermal pyrolysis of Samanea saman seeds towards the production of renewable fuel. *J Energy Inst* 93(3):1148–1162
- Mishra RK, Mohanty K (2018) Thermocatalytic conversion of non-edible Neem seeds towards clean fuel and chemicals. *J Anal Appl Pyrol* 134:83–92
- Van der Stelt M et al (2011) Biomass upgrading by torrefaction for the production of biofuels: A review. *Biomass Bioenerg* 35(9):3748–3762
- Chatterjee R et al (2020) Effect of pyrolysis temperature on physicochemical properties and acoustic-based amination of biochar for efficient CO₂ adsorption. *Front Energy Res* 8:85
- Codou A et al (2021) Impact of temperature and in situ FeCo catalysis on the architecture and Young's modulus of model wood-based biocarbon. *Green Chem* 23:3015–3027
- Liu W-J, Jiang H, Yu H-Q (2015) Development of biochar-based functional materials: toward a sustainable platform carbon material. *Chem Rev* 115(22):12251–12285
- Wang J, Wang S (2019) Preparation, modification and environmental application of biochar: a review. *J Clean Prod* 227:1002–1022
- Rawat J, Saxena J, Sanwal P (2019) Biochar: a sustainable approach for improving plant growth and soil properties. In *Biochar-An imperative amendment for soil and the environment*. IntechOpen, pp 1–17
- Ogunsona EO et al (2018) Thermally stable pyrolytic biocarbon as an effective and sustainable reinforcing filler for polyamide bio-composites fabrication. *J Polym Environ* 26(9):3574–3589
- Lehmann J (2007) Biochar for mitigating climate change: carbon sequestration in the black. In *Forum Geöökologie*
- Nhuchhen DR, Afzal MT (2017) HHV predicting correlations for torrefied biomass using proximate and ultimate analyses. *Bioengineering* 4(1):7
- Arnold S et al (2018) Slow pyrolysis of bio-oil and studies on chemical and physical properties of the resulting new bio-carbon. *J Clean Prod* 172:2748–2758
- Mishra RK, Mohanty K (2021) Fuel properties and compositional analysis of Areca catechu sawdust over MgO and ZSM-5 catalysts. *J Energy Inst* 94:252–262
- Mishra RK, Mohanty K (2019) Thermal and catalytic pyrolysis of pine sawdust (*Pinus ponderosa*) and Gulmohar seed (*Delonix regia*) towards production of fuel and chemicals. *Mater Sci Energy Technol* 2(2):139–149
- Khaksar L, Shirokoff J (2017) Effect of elemental sulfur and sulfide on the corrosion behavior of Cr-Mo low alloy steel for tubing and tubular components in oil and gas industry. *Materials* 10(4):430
- Mishra RK, Muraraka A, Mohanty K (2020) Optimization of process parameters and catalytic pyrolysis of Cascabela thevetia seeds over low-cost catalysts towards renewable fuel production. *J Energy Inst* 93(5):2033–2043
- Mishra RK, Mohanty K (2020) Effect of low-cost catalysts on yield and properties of fuel from waste biomass for hydrocarbon-rich oil production. *Mater Sci Energy Technol* 3:526–535
- Lu Q et al (2010) Catalytic upgrading of biomass fast pyrolysis vapors with nano metal oxides: an analytical Py-GC/MS study. *Energies* 3(11):1805–1820
- Hidayat S et al (2018) Characterisation and Py-GC/MS analysis of Imperata Cylindrica as potential biomass for bio-oil production in Brunei Darussalam. *J Anal Appl Pyrol* 134:510–519
- Xiu S et al (2012) Pyrolysis and combustion characteristics of Bio-oil from swine manure. *J Therm Anal Calorim* 107(2):823–829
- Mishra RK, Mohanty K (2020) Pyrolysis of Manilkara zapota seeds over ZSM-5 to produce high-quality bio-oil and chemicals. *Fuel* 280:118594
- Xiu S, Shahbazi A (2012) Bio-oil production and upgrading research: A review. *Renew Sustain Energy Rev* 16(7):4406–4414
- Väisänen T et al (2018) A rapid technique for monitoring volatile organic compound emissions from wood–plastic composites. *Indoor Built Environ* 27(2):194–204
- Li Z et al (2020) Characterization of Chicken Feather Biocarbon for Use in Sustainable Biocomposites. *Front Mater* 7:3
- Watt E et al (2020) Hybrid biocomposites from polypropylene, sustainable biocarbon and graphene nanoplatelets. *Sci Rep* 10(1):1–13
- Mishra RK, Mohanty K (2019) Pyrolysis of three waste biomass: Effect of biomass bed thickness and distance between successive beds on pyrolytic products yield and properties. *Renew Energy* 141:549–558
- Stankovikj F et al (2017) Evolution of functional groups during pyrolysis oil upgrading. *Energy Fuels* 31(8):8300–8316

37. Mishra A et al (2020) Extensive thermogravimetric and thermo-kinetic study of waste motor oil based on iso-conversional methods. *Energy Convers Manage* 221:113194
38. Chukwunke J et al (2016) Production by pyrolysis and analysis of bio-oil from mahogany wood (*Swietenia macrophylla*). *Brit J Appl Sci Technol* 17:1–9
39. Mishra RK, Mohanty K (2021) Kinetic analysis and pyrolysis behavior of low-value waste lignocellulosic biomass for its bio-energy potential using thermogravimetric analyzer. *Mater Sci Energy Technol* 4:136–147
40. Asadullah M et al (2013) Production and detailed characterization of bio-oil from fast pyrolysis of palm kernel shell. *Biomass Bioenerg* 59:316–324
41. Ren X et al (2017) The preparation and characterization of pyrolysis bio-oil-resorcinol-aldehyde resin cold-set adhesives for wood construction. *Polymers* 9(6):232
42. Titiladunayo IF, McDonald AG, Fapetu OP (2012) Effect of temperature on biochar product yield from selected lignocellulosic biomass in a pyrolysis process. *Waste Biomass Valorization* 3(3):311–318
43. Debiagi PEA et al (2017) Algae characterization and multistep pyrolysis mechanism. *J Anal Appl Pyrol* 128:423–436
44. Edreis EM, Yao H (2016) Kinetic thermal behaviour and evaluation of physical structure of sugar cane bagasse char during non-isothermal steam gasification. *J Market Res* 5(4):317–326
45. Fu P et al (2011) Effect of temperature on gas composition and char structural features of pyrolyzed agricultural residues. *Biores Technol* 102(17):8211–8219
46. Rafiq MK et al (2016) Influence of pyrolysis temperature on physico-chemical properties of corn stover (*Zea mays L.*) biochar and feasibility for carbon capture and energy balance. *PLoS one* 11(6):e0156894
47. Keiluweit M et al (2010) Dynamic molecular structure of plant biomass-derived black carbon (biochar). *Environ Sci Technol* 44(4):1247–1253
48. Mimmo T et al (2014) Effect of pyrolysis temperature on miscanthus (*Miscanthus × giganteus*) biochar physical, chemical and functional properties. *Biomass Bioenerg* 62:149–157
49. Mishra RK, Mohanty K (2021) Bio-oil and biochar production using thermal and catalytic pyrolysis of low-value waste neem seeds over low-cost catalysts: effects of operating conditions on product yields and studies of physicochemical characteristics of bio-oil and biochar. *Biochar*:1–16
50. Major I et al (2018) Graphitization of *Miscanthus* grass biocarbon enhanced by in situ generated FeCo nanoparticles. *Green Chem* 20(10):2269–2278
51. Li X, Hayashi J-I, Li C-Z (2006) FT-Raman spectroscopic study of the evolution of char structure during the pyrolysis of a Victorian brown coal. *Fuel* 85(12–13):1700–1707
52. Zhang J et al (2009) Effect of growing CNTs onto bamboo charcoals on adsorption of copper ions in aqueous solution. *Langmuir* 25(1):269–274
53. Kwon JH et al (2013) Effect of carbonization temperature on electrical resistivity and physical properties of wood and wood-based composites. *Compos B Eng* 46:102–107
54. Hoffmann V et al (2019) Study of the electrical conductivity of biobased carbonaceous powder materials under moderate pressure for the application as electrode materials in energy storage technologies. *Gcb Bioenergy* 11(1):230–248
55. Snowdon MR, Mohanty AK, Misra M (2014) A study of carbonized lignin as an alternative to carbon black. *ACS Sustain Chem Eng* 2(5):1257–1263
56. Celzard A et al (2002) Electrical conductivity of carbonaceous powders. *Carbon* 40(15):2801–2815
57. Smith W, Wilkes G (1944) Thermal conductivity of carbon blacks. *Ind Eng Chem* 36(12):1111–1112
58. Balandin AA (2011) Thermal properties of graphene and nano-structured carbon materials. *Nat Mater* 10(8):569–581
59. Yargicoglu EN et al (2015) Physical and chemical characterization of waste wood derived biochars. *Waste Manag* 36:256–268

Publisher's note Springer Nature remains neutral with regard to jurisdictional claims in published maps and institutional affiliations.